

Direction Reconstruction using a CNN for GeV-Scale Neutrinos in IceCube

The IceCube Collaboration

(a complete list of authors can be found at the end of the proceedings)

E-mail: shiqi.yu@icecube.wisc.edu

The IceCube Neutrino Observatory observes neutrinos interacting deep within the South Pole ice. It consists of 5,160 digital optical modules, which are embedded within a cubic kilometer of ice, over depths of 1,450 m to 2,450 m. At the lower center of the array is the DeepCore subdetector. Its denser sensor configuration lowers the observable energy threshold to the GeV-scale, facilitating the study of atmospheric neutrino oscillations. The precise reconstruction of neutrino direction is critical in the measurements of oscillation parameters. This work presents a method to reconstruct the zenith angle of GeV-scale events in IceCube by using a convolutional neural network and compares the result to that of the current likelihood-based reconstruction algorithm.

Corresponding authors: Shiqi Yu¹*

¹ *Michigan State University*

* Presenter

37th International Cosmic Ray Conference (ICRC 2021)

July 12th – 23rd, 2021

Online – Berlin, Germany

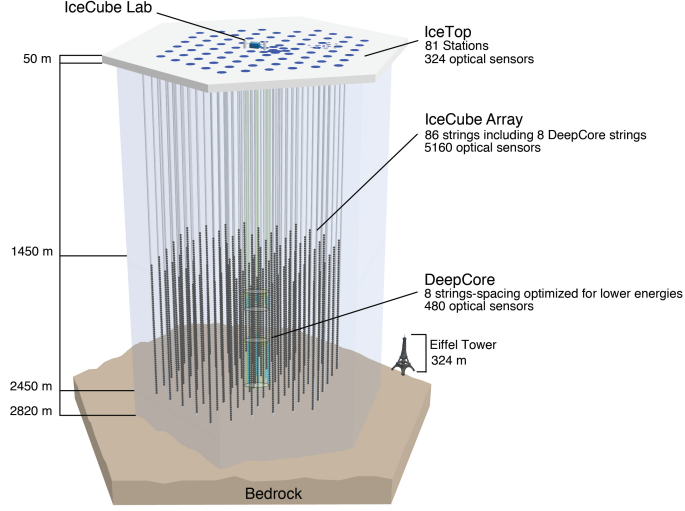


Figure 1: IceCube Neutrino Observatory at the South Pole

1. IceCube Neutrino Observatory

IceCube Neutrino Observatory is a Cherenkov detector located at the South Pole. As shown in Figure 1, there are 5,160 digital optical modules (DOMs) deployed in the ice which make up of 78 IceCube strings and 8 DeepCore strings each containing 60 DOMs. The IceCube strings are arranged approximately 125 m apart with the DOMs spacing as 17 m. The DeepCore strings are located at the lower center of the IceCube string array with a denser configuration using DOMs with a (35%) higher quantum efficiency. The ten layers of DeepCore DOMs closest to the surface provide a veto on cosmic-ray muons which is an abundant background in the IceCube oscillation analyses. The DeepCore sub-detector lowers the energy threshold from several TeV down to approximately 5 GeV, allowing the study of neutrino oscillation in IceCube.

2. Neutrino Oscillation

The DeepCore sub-detector provides sensitivity to atmospheric mixing parameters, the mixing angle (θ_{23}) and mass splitting (Δm_{32}^2). These can be measured by studying ν_μ disappearance using atmospheric neutrinos that are created by cosmic rays interacting with the atmosphere.

Neutrinos are produced and detected as electron (ν_e), muon (ν_μ), or tau (ν_τ) neutrinos, while they propagate in three mass eigenstates: ν_1 , ν_2 , and ν_3 . They can be produced in one flavor state but detected having a different flavor, which is called neutrino oscillations. ν_μ disappearance is measured in the deficits of the $\nu_\mu \rightarrow \nu_\mu$ flux, the survival probability of which is described by

$$P(\nu_\mu \rightarrow \nu_\mu) \approx 1 - \sin^2(2\theta_{23}) \sin^2\left(\frac{1.27\Delta m_{32}^2 L}{E}\right), \quad (1)$$

where L represents neutrino distance of travel; E represents neutrino energy; and θ_{23} is the mixing angle and $\Delta m_{32}^2 \equiv m_3^2 - m_2^2$ is the squared-mass difference between neutrino mass states ν_3 and ν_2 . L can not be directly known, but it can be inferred using incident neutrino zenith angle (θ_{zenith}).

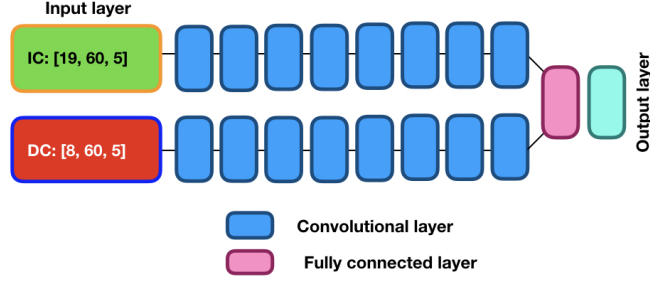


Figure 2: Structure of CNN with input shape of (number of strings, 60 DOMs, 5 variables), where DC represents 8 DeepCore strings and IC represents 19 nearby IceCube strings

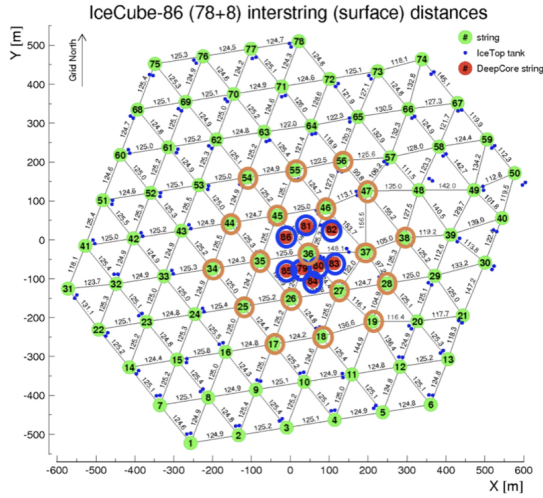


Figure 3: Top view of 8 DeepCore strings (red filled) and 19 IceCube strings (orange circled) used by CNN

When neutrinos interact within the detector, relativistic charged particles are produced, emitting Cherenkov photons which are detected by the DOMs and converted into series of electrical pulses. Precisely measuring neutrino θ_{zenith} is critical in measuring oscillation parameters. A convolutional network (CNN) is employed to reconstruct θ_{zenith} by using the series of electrical pulses of neutrino events.

3. Method of Reconstruction

CNNs are broadly used in modern physics experiments for particle identification [1] and reconstruction [2] [3]. The CNN employed for θ_{zenith} reconstruction has the structure as shown in Figure 2.

There are two sub-networks each of which consists of 8 convolutional layers. Each convolutional layer extracts some features from the input images and creates the output images which are used as the input to the following layer. The training samples are fed into the CNN via two input layers: one is for the 8 DeepCore strings; another is for the 19 surrounding IceCube strings, as shown in Figure 3. For each DOM on all the strings, 5 variables are calculated using the pulse

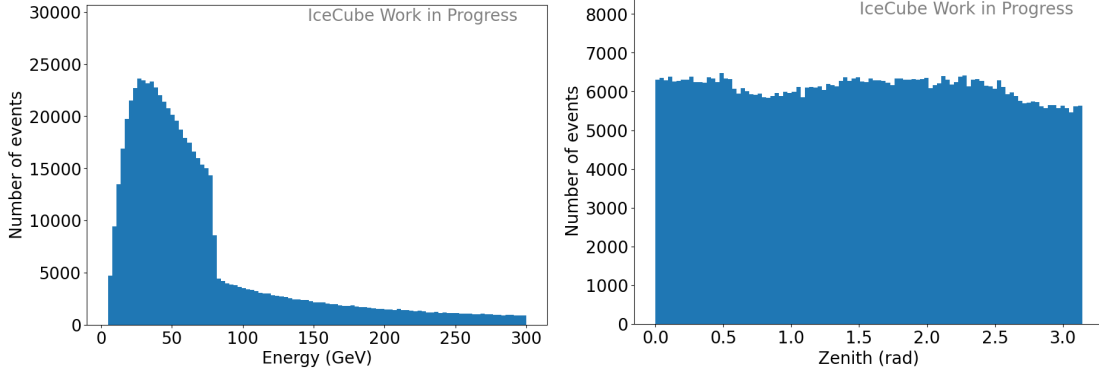


Figure 4: Unweighted true energy (left) and θ_{zenith} (right) distributions of training dataset

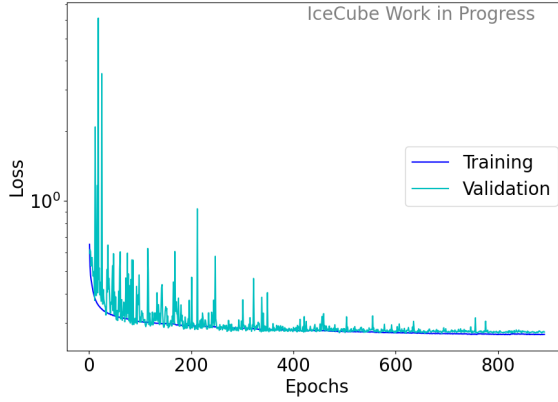


Figure 5: Training (blue) and validation (teal) loss curves

series of the DOM: sum of charges, time of the first hit, time of the last hit, charge weighted mean of pulse time, and charge weighted standard deviation of pulse time. The output layer delivers the value of θ_{zenith} in the range of $(0, \pi)$.

The training sample is simulated ν_{μ} charged-current (CC) Monte-Carlo (MC) dataset with a flat θ_{zenith} distribution and energy between 5-300 GeV, as shown in Figure 4. A total of 5,024,876 simulated events were used to train the CNN, of which 80% were used as a training set and 20% for validation. The CNN was trained on the high performance computing at ICER, requiring approximately 6 days and over 800 epochs to converge. At the end of each epoch, the CNN updates all the parameters to minimize a loss function, defined as

$$\text{loss} = \sum_i \hat{\theta}_{\text{zenith}}(i) - \theta_{\text{zenith}}(i), \quad (2)$$

where i represents event in validation dataset, $\hat{\theta}_{\text{zenith}}(i)$ represents the CNN predicted θ_{zenith} value of event i , and $\theta_{\text{zenith}}(i)$ represents the true θ_{zenith} value of event i . The training and validation loss curves are shown in Figure 5.

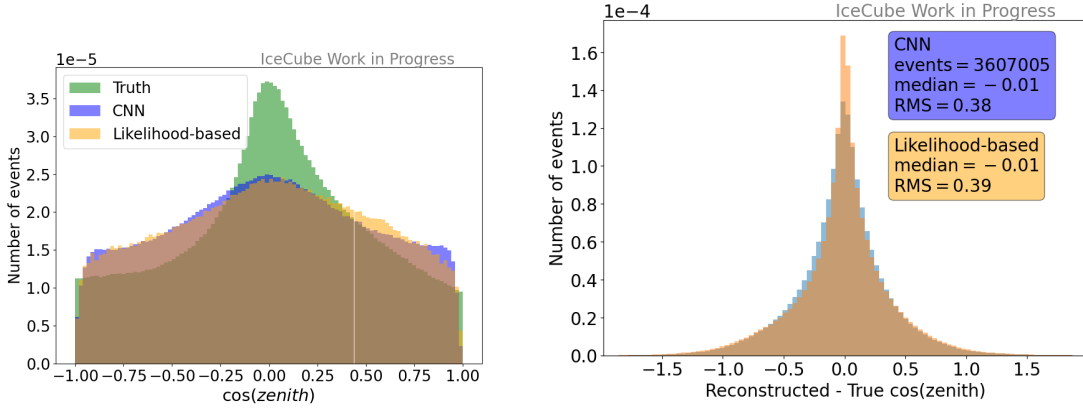


Figure 6: 1D distributions of $\cos(\theta_{\text{zenith}})$ (left) and $\cos(\theta_{\text{zenith}})$ reconstruction error (right) with blue (orange) representing CNN (likelihood-based) reconstructed $\cos(\theta_{\text{zenith}})$ and green representing true $\cos(\theta_{\text{zenith}})$ of true ν_{μ} CC events.

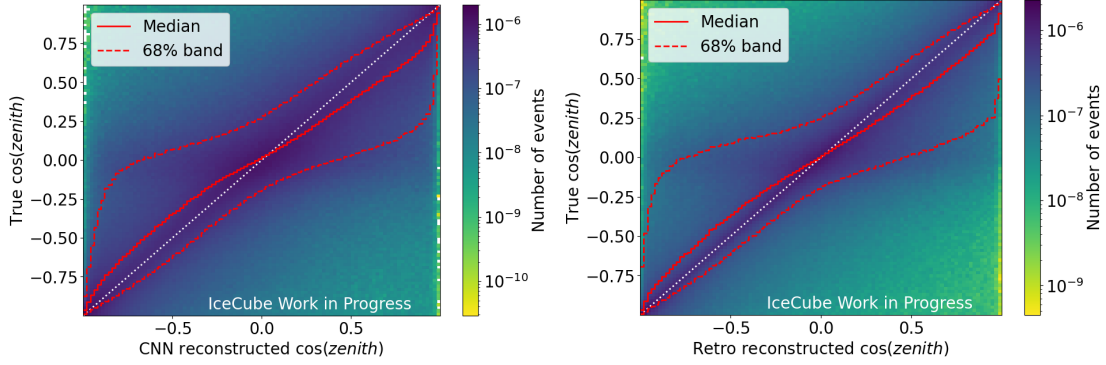


Figure 7: 2D distributions of true vs. CNN (left) or likelihood-based (right) reconstructed $\cos(\theta_{\text{zenith}})$ with median (solid) and contours (dashed) of 68% of events in vertical slices

4. Results

To show the performance of the CNN predicted θ_{zenith} , a standard likelihood-based reconstruction method is used as comparison. The official ν_{μ} and ν_e CC MC files are used to evaluate the results of these two reconstruction methods. Selections based on the interacting point position (vertex) and energy of neutrino events that are reconstructed by the likelihood-based method are applied. These selections are inherited from the current oscNext analysis where they are optimized for neutrino oscillation signal efficiency. These likelihood-based selections are reconstructed: neutrino energy in range of $[5, 300]$ GeV, z -coordinate of neutrino event vertex in range of $[-500, -200]$ m, and $\rho_{36} < 300$ m, where ρ_{36} represents radius of neutrino vertex relative to IC string 36.

4.1 ν_{μ} CC sample

The plots in Figure 6 show the 1D distributions of $\cos(\theta_{\text{zenith}})$. The CNN and likelihood-based methods have similar spectral shapes and both reconstructed $\cos(\theta_{\text{zenith}})$ values are smeared to the higher (lower) values at the lower (higher) boundary.

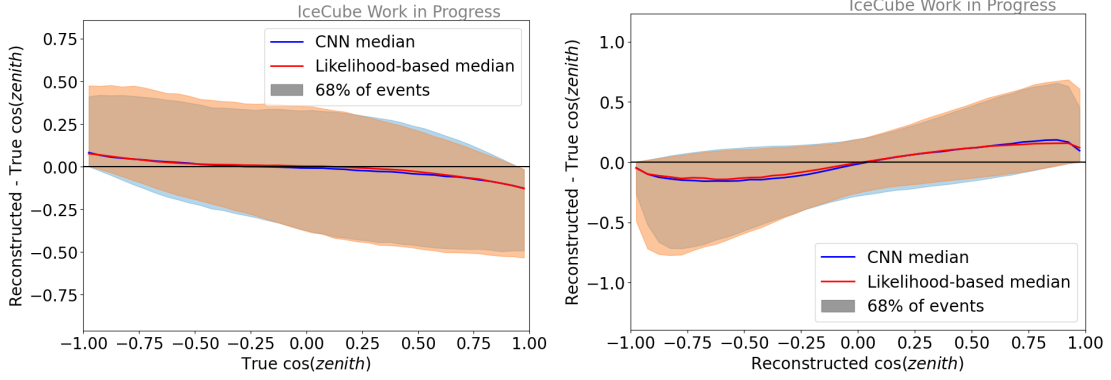


Figure 8: 1D slices of reconstructed - true vs. true (left) or reconstructed (right) $\cos(\theta_{zenith})$ with blue (orange) representing CNN (likelihood-based) result, solid curve representing median, and shaded area containing 68% of events

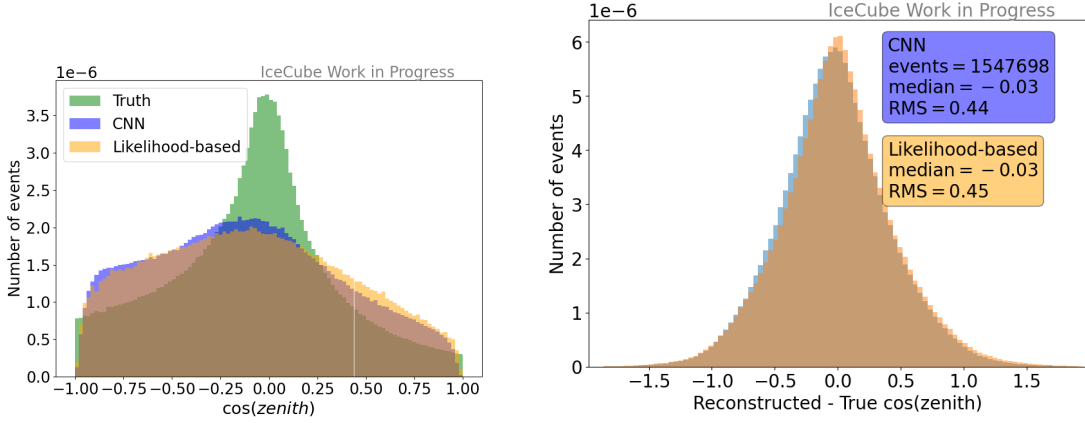


Figure 9: 1D distributions of $\cos(\theta_{zenith})$ (left) reconstructed - true $\cos(\theta_{zenith})$ (right) with blue (orange) representing CNN (likelihood-based) reconstructed $\cos(\theta_{zenith})$ and green representing true $\cos(\theta_{zenith})$ of true ν_e CC events

The 2D distributions of true versus reconstructed $\cos(\theta_{zenith})$ are shown in Figure 7. Ideally, the median curve of the distribution should approach the diagonal white dot line, which represents the 1:1 ratio of true:reconstructed $\cos(\theta_{zenith})$ and the contours of 68% of events should be narrowly parallel to the median curve. In the 2D distributions of the CNN and likelihood-based methods, both the medians and 68%-contours are comparable.

As shown in Figure 6, the overall RMS of CNN method is smaller than that of the likelihood-based method by 2.6%. As shown in Figure 8, plotting bias against true or reconstructed $\cos(\theta_{zenith})$ shows that the performances of CNN and likelihood-based methods are similarly well.

4.2 ν_e CC sample

In Figure 9, the 1D distributions of $\cos(\theta_{zenith})$ of the CNN and likelihood-based methods have similar spectral shapes. The 2D distributions of true vs. reconstructed $\cos(\theta_{zenith})$ (see Figure 10) look similar to each other while both having wider 68%-contours than those of the ν_μ CC events. This is as expected: most of the ν_μ CC events are track-like in the IceCube detector and easier to

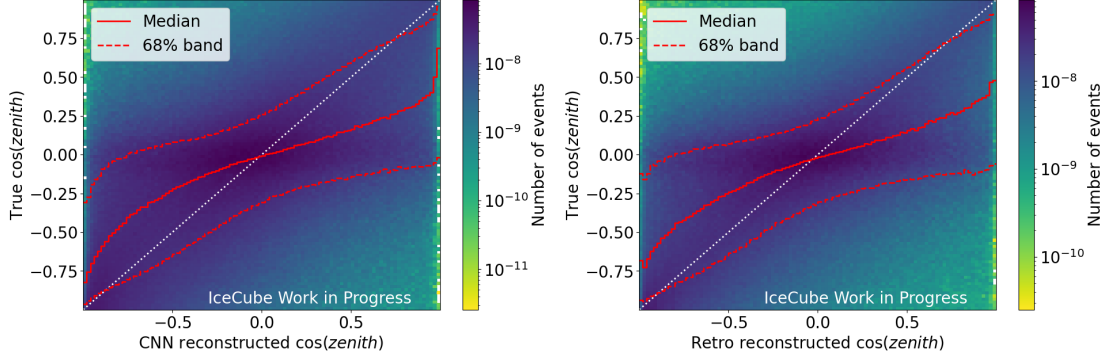


Figure 10: 2D distributions of true vs. CNN (left) or likelihood-based (right) reconstructed $\cos(\theta_{zenith})$ with median (solid) and contours (dashed) of 68% of events plotted on the top

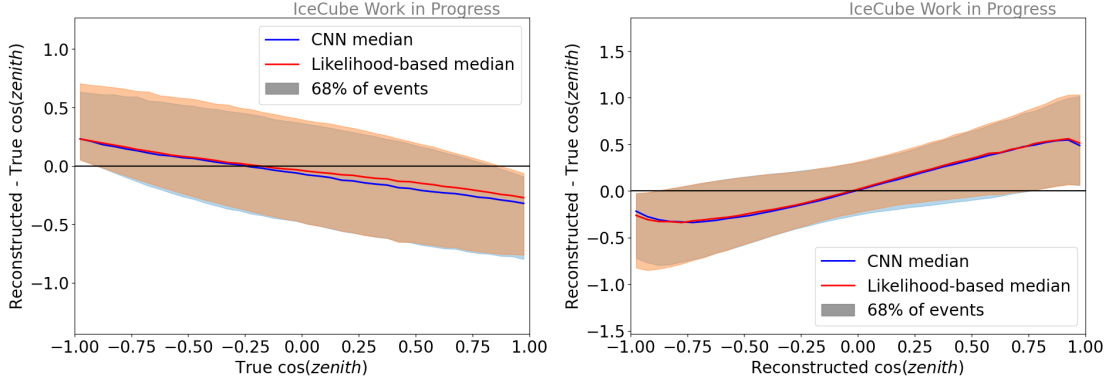


Figure 11: 1D slices of reconstructed - true vs. true (left) or reconstructed (right) $\cos(\theta_{zenith})$ with blue (orange) representing CNN (likelihood-based) result, solid curve representing median, and shaded area containing 68% of events

reconstruct than the cascade-like ν_e CC events. This is also the reason that the bias distributions are wider and RMS values are larger in Figure 9 compared to those of the true ν_μ CC events in Figure 6.

Similarly, as shown in the bias vs. true or reconstructed $\cos(\theta_{zenith})$ slices (see Figure 11), the performance of the CNN method is comparable to that of the likelihood-based method, while both methods have worse performances than those of the ν_μ CC events.

4.3 Processing speed

As listed in Table 1, the likelihood-based method can only use CPU clusters while the CNN method can run on both CPU and GPU. The CNN benefits from parallel processing and is 10,000 times faster than the current method when run on a K80 GPU. Even if both methods are evaluated on the same CPU, running the CNN method is still over 400 times faster than running the likelihood-based method. Rapid processing is crucial for analyses using large data sets as is generally true of high energy physics experiments.

Second/Event	GPU	CPU
CNN	0.0044	0.108
Likelihood-based	–	44.97

Table 1: Processing speed of CNN and likelihood-based methods

5. Conclusion

The CNN method trained on the simulated low-energy ν_μ CC sample with a flat neutrino direction distribution provides a comparable performance to the current likelihood-based method, improving the overall RMS in the direction reconstruction by 2.6% on the ν_μ sample and 2.2% on the ν_e events. The bias against either true or reconstructed $\cos(\theta_{\text{zenith}})$ slices are robust and comparable between the two methods. Using GPU resources, the CNN method is 10,000 times faster than the current method in processing events, easing the computational burden required for future oscillation analyses with DeepCore.

6. Acknowledgement

This study is supported by National Science Foundation under grant number: NSF1913607. Any opinions, findings, or conclusions stated in this proceeding are only those of the author(s); and do not necessarily reflect the views of the National Science Foundation. Additional acknowledgements for the collaboration are included seperated.

References

- [1] A. A. et el. *JINST* **11** (2016) P09001.
- [2] IceCube Collaboration, M. Huennefeld *EPJ Web of Conferences* **207** (2019) 05005.
- [3] IceCube Collaboration, J. Micallef *PoS ICRC2021* (2021) 1053.

Full Author List: IceCube Collaboration

R. Abbasi¹⁷, M. Ackermann⁵⁹, J. Adams¹⁸, J. A. Aguilar¹², M. Ahlers²², M. Ahrens⁵⁰, C. Alispach²⁸, A. A. Alves Jr.³¹, N. M. Amin⁴², R. An¹⁴, K. Andeen⁴⁰, T. Anderson⁵⁶, G. Anton²⁶, C. Argüelles¹⁴, Y. Ashida³⁸, S. Axani¹⁵, X. Bai⁴⁶, A. Balagopal V.³⁸, A. Barbano²⁸, S. W. Barwick³⁰, B. Bastian⁵⁹, V. Basu³⁸, S. Baur¹², R. Bay⁸, J. J. Beatty^{20,21}, K.-H. Becker⁵⁸, J. Becker Tjus¹¹, C. Bellenghi²⁷, S. BenZvi⁴⁸, D. Berley¹⁹, E. Bernardini^{59,60}, D. Z. Besson^{34,61}, G. Binder^{8,9}, D. Bindig⁵⁸, E. Blaufuss¹⁹, S. Blot⁵⁹, M. Boddenberg¹, F. Bontempo³¹, J. Borowka¹, S. Böser³⁹, O. Botner⁵⁷, J. Böttcher¹, E. Bourbeau²², F. Bradascio⁵⁹, J. Braun³⁸, S. Bron²⁸, J. Brostean-Kaiser⁵⁹, S. Browne³², A. Burgman⁵⁷, R. T. Burley², R. S. Busse⁴¹, M. A. Campana⁴⁵, E. G. Carnie-Bronca², C. Chen⁶, D. Chirkin³⁸, K. Choi⁵², B. A. Clark²⁴, K. Clark³³, L. Classen⁴¹, A. Coleman⁴², G. H. Collin¹⁵, J. M. Conrad¹⁵, P. Coppin¹³, P. Correa¹³, D. F. Cowen^{55,56}, R. Cross⁴⁸, C. Dappen¹, P. Dave⁶, C. De Clercq¹³, J. J. DeLaunay⁵⁶, H. Dembinski⁴², K. Deoskar⁵⁰, S. De Ridder²⁹, A. Desai³⁸, P. Desiati³⁸, K. D. de Vries¹³, G. de Wasseige¹³, M. de With¹⁰, T. DeYoung²⁴, S. Dharani¹, A. Diaz¹⁵, J. C. Díaz-Vélez³⁸, M. Dittmer⁴¹, H. Dujmovic³¹, M. Dunkman⁵⁶, M. A. DuVernois³⁸, E. Dvorak⁴⁶, T. Ehrhardt³⁹, P. Eller²⁷, R. Engel^{31,32}, H. Erpenbeck¹, J. Evans¹⁹, P. A. Evenson⁴², K. L. Fan¹⁹, A. R. Fazely⁷, S. Fiedlschuster²⁶, A. T. Fienberg⁵⁶, K. Filimonov⁸, C. Finley⁵⁰, L. Fischer⁵⁹, D. Fox⁵⁵, A. Frankowski^{11,59}, E. Friedman¹⁹, A. Fritz³⁹, P. Fürst¹, T. K. Gaisser⁴², J. Gallagher³⁷, E. Ganster¹, A. Garcia¹⁴, S. Garrappa⁵⁹, L. Gerhardt⁹, A. Ghadimi⁵⁴, C. Glaser⁵⁷, T. Glauch²⁷, T. Glüsenskamp²⁶, A. Goldschmidt⁹, J. G. Gonzalez⁴², S. Goswami⁵⁴, D. Grant²⁴, T. Grégoire⁵⁶, S. Griswold⁴⁸, M. Gündüz¹¹, C. Günther¹, C. Haack²⁷, A. Hallgren⁵⁷, R. Halliday²⁴, L. Halve¹, F. Halzen³⁸, M. Ha Minh²⁷, K. Hanson³⁸, J. Hardin³⁸, A. A. Harnisch²⁴, A. Haungs³¹, S. Hauser¹, D. Hebecker¹⁰, K. Helbing⁵⁸, F. Henningsen²⁷, E. C. Hettinger²⁴, S. Hickford⁵⁸, J. Hignight²⁵, C. Hill¹⁶, G. C. Hill², K. D. Hoffman¹⁹, R. Hoffmann⁵⁸, T. Hoinka²³, B. Hokanson-Fasig³⁸, K. Hoshina^{38,62}, F. Huang⁵⁶, M. Huber²⁷, T. Huber³¹, K. Hultqvist⁵⁰, M. Hünnefeld²³, R. Hussain³⁸, S. In⁵², N. Iovine¹², A. Ishihara¹⁶, M. Jansson⁵⁰, G. S. Japaridze⁵, M. Jeong⁵², B. J. P. Jones⁴, D. Kang³¹, W. Kang⁵², X. Kang⁴⁵, A. Kappes⁴¹, D. Kappesser³⁹, T. Karg⁵⁹, M. Kar²⁷, A. Karle³⁸, U. Katz²⁶, M. Kauze³⁸, M. Kellermann¹, J. L. Kelley³⁸, A. Kheirandish⁵⁶, K. Kin¹⁶, T. Kintscher⁵⁹, J. Kiryluk⁵¹, S. R. Klein^{8,9}, R. Koirala⁴², H. Kolanoski¹⁰, T. Kontrimas²⁷, L. Köpke³⁹, C. Kopper²⁴, S. Kopper⁵⁴, D. J. Koskinen²², P. Koundal³¹, M. Kovacevich⁴⁵, M. Kowalski^{10,59}, T. Kozynets²², E. Kun¹¹, N. Kurahashi⁴⁵, N. Lad⁵⁹, C. Lagunas Gualda⁵⁹, J. L. Lanfranchi⁵⁶, M. J. Larson¹⁹, F. Lauber⁵⁸, J. P. Lazar^{14,38}, J. W. Lee⁵², K. Leonard³⁸, A. Leszczyńska³², Y. Li⁵⁶, M. Lincetto¹¹, Q. R. Liu³⁸, M. Liubarska²⁵, E. Lohfink³⁹, C. J. Lozano Mariscal⁴¹, L. Lu³⁸, F. Lucarelli²⁸, A. Ludwig^{24,35}, W. Luszczak³⁸, Y. Lyu^{8,9}, W. Y. Ma⁵⁹, J. Madsen³⁸, K. B. M. Mahn²⁴, Y. Makino³⁸, S. Mancina³⁸, I. C. Mariş¹², R. Maruyama⁴³, K. Mase¹⁶, T. McElroy²⁵, F. McNally³⁶, J. V. Mead²², K. Meagher³⁸, A. Medina²¹, M. Meier¹⁶, S. Meighen-Berger²⁷, J. Micaller²⁴, D. Mockler¹², T. Montaruli²⁸, R. W. Moore²⁵, R. Morse³⁸, M. Moulai¹⁵, R. Naab⁵⁹, R. Nagai¹⁶, U. Naumann⁵⁸, J. Necker⁵⁹, L. V. Nguyen²⁴, H. Niederhausen²⁷, M. U. Nisa²⁴, S. C. Nowicki²⁴, D. R. Nygren⁹, A. Obertacke Pollmann⁵⁸, M. Oehler³¹, A. Olivas¹⁹, E. O'Sullivan⁵⁷, H. Pandya⁴², D. V. Pankova⁵⁶, N. Park³³, G. K. Parker⁴, E. N. Paudel⁴², L. Paul⁴⁰, C. Pérez de los Heros⁵⁷, L. Peters¹, J. Peterson³⁸, S. Philippen¹, D. Pieloth²³, S. Pieper⁵⁸, M. Pittermann³², A. Pizzuto³⁸, M. Plum⁴⁰, Y. Popovych³⁹, A. Porcelli²⁹, M. Prado Rodriguez³⁸, P. B. Price⁸, B. Pries²⁴, G. T. Przybylski⁹, C. Raab¹², A. Raisi¹⁸, M. Rameez²², K. Rawlins³, I. C. Rea²⁷, A. Rehman⁴², P. Reichherzer¹¹, R. Reimann¹, G. Renzi¹², E. Resconi²⁷, S. Reusch⁵⁹, W. Rhode²³, M. Richman⁴⁵, B. Riedel³⁸, E. J. Roberts², S. Robertson^{8,9}, G. Roellinghoff⁵², M. Rongen³⁹, C. Rott^{49,52}, T. Ruhe²³, D. Ryckbosch²⁹, D. Rysewyk Cantu²⁴, I. Safa^{14,38}, J. Saffer³², S. E. Sanchez Herrera²⁴, A. Sandrock²³, J. Sandroos³⁹, M. Santander⁵⁴, S. Sarkar⁴⁴, S. Sarkar²⁵, K. Satalecka⁵⁹, M. Scharf¹, L. V. Schaufel¹, H. Schieler³¹, S. Schindler²⁶, P. Schlunder²³, T. Schmidt¹⁹, A. Schneider³⁸, J. Schneider²⁶, F. G. Schröder^{31,42}, L. Schumacher²⁷, G. Schwefer¹, S. Sclafani⁴⁵, D. Seckel⁴², S. Seunarine⁴⁷, A. Sharma⁵⁷, S. Shefali³², M. Silva³⁸, B. Skrzypek¹⁴, B. Smithers⁴, R. Snihur³⁸, J. Soedingrekso²³, D. Soldin⁴², C. Spannfellner²⁷, G. M. Spiczak⁴⁷, C. Spiering^{59,61}, J. Stachurska⁵⁹, M. Stamatikos²¹, T. Stanev⁴², R. Stein⁵⁹, J. Stettner¹, A. Steuer³⁹, T. Stezelberger⁹, T. Stürwald⁵⁸, T. Stuttard²², G. W. Sullivan¹⁹, I. Taboada⁶, F. Tenholt¹¹, S. Ter-Antonyan⁷, S. Tilav⁴², F. Tischbein¹, K. Tollefson²⁴, L. Tomankova¹¹, C. Tönnis⁵³, S. Toscano¹², D. Tosi³⁸, A. Trettin⁵⁹, M. Tselengidou²⁶, C. F. Tung⁶, A. Turcati²⁷, R. Turcotte³¹, C. F. Turley⁵⁶, J. P. Twagirayezu²⁴, B. Ty³⁸, M. A. Unlad Elorrieta⁴¹, N. Valtonen-Mattila⁵⁷, J. Vandenbroucke³⁸, N. van Eijndhoven¹³, D. Vannerom¹⁵, J. van Santen⁵⁹, S. Verpoest²⁹, W. Vraeghe²⁹, C. Walck⁵⁰, T. B. Watson⁴, C. Weaver²⁴, P. Weigel¹⁵, A. Weindl³¹, M. J. Weiss⁵⁶, J. Weldert³⁹, C. Wendt³⁸, J. Werthebach²³, M. Weyrauch³², N. Whitehorn^{24,35}, C. H. Wiebusch¹, D. R. Williams⁵⁴, M. Wolf²⁷, K. Woschnagg⁸, G. Wrede²⁶, J. Wulf¹¹, X. W. Xu⁷, Y. Xu⁵¹, J. P. Yanez²⁵, S. Yoshida¹⁶, S. Yu²⁴, T. Yuan³⁸, Z. Zhang⁵¹

¹ III. Physikalisches Institut, RWTH Aachen University, D-52056 Aachen, Germany

² Department of Physics, University of Adelaide, Adelaide, 5005, Australia

³ Dept. of Physics and Astronomy, University of Alaska Anchorage, 3211 Providence Dr., Anchorage, AK 99508, USA

⁴ Dept. of Physics, University of Texas at Arlington, 502 Yates St., Science Hall Rm 108, Box 19059, Arlington, TX 76019, USA

⁵ CTSPPS, Clark-Atlanta University, Atlanta, GA 30314, USA

⁶ School of Physics and Center for Relativistic Astrophysics, Georgia Institute of Technology, Atlanta, GA 30332, USA

⁷ Dept. of Physics, Southern University, Baton Rouge, LA 70813, USA

⁸ Dept. of Physics, University of California, Berkeley, CA 94720, USA

⁹ Lawrence Berkeley National Laboratory, Berkeley, CA 94720, USA

¹⁰ Institut für Physik, Humboldt-Universität zu Berlin, D-12489 Berlin, Germany

¹¹ Fakultät für Physik & Astronomie, Ruhr-Universität Bochum, D-44780 Bochum, Germany

¹² Université Libre de Bruxelles, Science Faculty CP230, B-1050 Brussels, Belgium

¹³ Vrije Universiteit Brussel (VUB), Dienst ELEM, B-1050 Brussels, Belgium

¹⁴ Department of Physics and Laboratory for Particle Physics and Cosmology, Harvard University, Cambridge, MA 02138, USA

¹⁵ Dept. of Physics, Massachusetts Institute of Technology, Cambridge, MA 02139, USA

- ¹⁶ Dept. of Physics and Institute for Global Prominent Research, Chiba University, Chiba 263-8522, Japan
¹⁷ Department of Physics, Loyola University Chicago, Chicago, IL 60660, USA
¹⁸ Dept. of Physics and Astronomy, University of Canterbury, Private Bag 4800, Christchurch, New Zealand
¹⁹ Dept. of Physics, University of Maryland, College Park, MD 20742, USA
²⁰ Dept. of Astronomy, Ohio State University, Columbus, OH 43210, USA
²¹ Dept. of Physics and Center for Cosmology and Astro-Particle Physics, Ohio State University, Columbus, OH 43210, USA
²² Niels Bohr Institute, University of Copenhagen, DK-2100 Copenhagen, Denmark
²³ Dept. of Physics, TU Dortmund University, D-44221 Dortmund, Germany
²⁴ Dept. of Physics and Astronomy, Michigan State University, East Lansing, MI 48824, USA
²⁵ Dept. of Physics, University of Alberta, Edmonton, Alberta, Canada T6G 2E1
²⁶ Erlangen Centre for Astroparticle Physics, Friedrich-Alexander-Universität Erlangen-Nürnberg, D-91058 Erlangen, Germany
²⁷ Physik-department, Technische Universität München, D-85748 Garching, Germany
²⁸ Département de physique nucléaire et corpusculaire, Université de Genève, CH-1211 Genève, Switzerland
²⁹ Dept. of Physics and Astronomy, University of Gent, B-9000 Gent, Belgium
³⁰ Dept. of Physics and Astronomy, University of California, Irvine, CA 92697, USA
³¹ Karlsruhe Institute of Technology, Institute for Astroparticle Physics, D-76021 Karlsruhe, Germany
³² Karlsruhe Institute of Technology, Institute of Experimental Particle Physics, D-76021 Karlsruhe, Germany
³³ Dept. of Physics, Engineering Physics, and Astronomy, Queen's University, Kingston, ON K7L 3N6, Canada
³⁴ Dept. of Physics and Astronomy, University of Kansas, Lawrence, KS 66045, USA
³⁵ Department of Physics and Astronomy, UCLA, Los Angeles, CA 90095, USA
³⁶ Department of Physics, Mercer University, Macon, GA 31207-0001, USA
³⁷ Dept. of Astronomy, University of Wisconsin–Madison, Madison, WI 53706, USA
³⁸ Dept. of Physics and Wisconsin IceCube Particle Astrophysics Center, University of Wisconsin–Madison, Madison, WI 53706, USA
³⁹ Institute of Physics, University of Mainz, Staudinger Weg 7, D-55099 Mainz, Germany
⁴⁰ Department of Physics, Marquette University, Milwaukee, WI, 53201, USA
⁴¹ Institut für Kernphysik, Westfälische Wilhelms-Universität Münster, D-48149 Münster, Germany
⁴² Bartol Research Institute and Dept. of Physics and Astronomy, University of Delaware, Newark, DE 19716, USA
⁴³ Dept. of Physics, Yale University, New Haven, CT 06520, USA
⁴⁴ Dept. of Physics, University of Oxford, Parks Road, Oxford OX1 3PU, UK
⁴⁵ Dept. of Physics, Drexel University, 3141 Chestnut Street, Philadelphia, PA 19104, USA
⁴⁶ Physics Department, South Dakota School of Mines and Technology, Rapid City, SD 57701, USA
⁴⁷ Dept. of Physics, University of Wisconsin, River Falls, WI 54022, USA
⁴⁸ Dept. of Physics and Astronomy, University of Rochester, Rochester, NY 14627, USA
⁴⁹ Department of Physics and Astronomy, University of Utah, Salt Lake City, UT 84112, USA
⁵⁰ Oskar Klein Centre and Dept. of Physics, Stockholm University, SE-10691 Stockholm, Sweden
⁵¹ Dept. of Physics and Astronomy, Stony Brook University, Stony Brook, NY 11794-3800, USA
⁵² Dept. of Physics, Sungkyunkwan University, Suwon 16419, Korea
⁵³ Institute of Basic Science, Sungkyunkwan University, Suwon 16419, Korea
⁵⁴ Dept. of Physics and Astronomy, University of Alabama, Tuscaloosa, AL 35487, USA
⁵⁵ Dept. of Astronomy and Astrophysics, Pennsylvania State University, University Park, PA 16802, USA
⁵⁶ Dept. of Physics, Pennsylvania State University, University Park, PA 16802, USA
⁵⁷ Dept. of Physics and Astronomy, Uppsala University, Box 516, S-75120 Uppsala, Sweden
⁵⁸ Dept. of Physics, University of Wuppertal, D-42119 Wuppertal, Germany
⁵⁹ DESY, D-15738 Zeuthen, Germany
⁶⁰ Università di Padova, I-35131 Padova, Italy
⁶¹ National Research Nuclear University, Moscow Engineering Physics Institute (MEPhI), Moscow 115409, Russia
⁶² Earthquake Research Institute, University of Tokyo, Bunkyo, Tokyo 113-0032, Japan

Acknowledgements

USA – U.S. National Science Foundation-Office of Polar Programs, U.S. National Science Foundation-Physics Division, U.S. National Science Foundation-EPSCoR, Wisconsin Alumni Research Foundation, Center for High Throughput Computing (CHTC) at the University of Wisconsin–Madison, Open Science Grid (OSG), Extreme Science and Engineering Discovery Environment (XSEDE), Frontera computing project at the Texas Advanced Computing Center, U.S. Department of Energy-National Energy Research Scientific Computing Center, Particle astrophysics research computing center at the University of Maryland, Institute for Cyber-Enabled Research at Michigan State University, and Astroparticle physics computational facility at Marquette University; Belgium – Funds for Scientific Research (FRS-FNRS and FWO), FWO Odysseus and Big Science programmes, and Belgian Federal Science Policy Office (Belspo); Germany – Bundesministerium für Bildung und Forschung (BMBF), Deutsche Forschungsgemeinschaft (DFG), Helmholtz Alliance for Astroparticle Physics (HAP), Initiative and Networking Fund of the Helmholtz Association, Deutsches Elektronen Synchrotron (DESY), and High Performance Computing cluster of the RWTH Aachen; Sweden – Swedish Research Council, Swedish Polar Research Secretariat, Swedish National Infrastructure for Computing (SNIC), and Knut and Alice Wallenberg Foundation; Australia – Australian

Research Council; Canada – Natural Sciences and Engineering Research Council of Canada, Calcul Québec, Compute Ontario, Canada Foundation for Innovation, WestGrid, and Compute Canada; Denmark – Villum Fonden and Carlsberg Foundation; New Zealand – Marsden Fund; Japan – Japan Society for Promotion of Science (JSPS) and Institute for Global Prominent Research (IGPR) of Chiba University; Korea – National Research Foundation of Korea (NRF); Switzerland – Swiss National Science Foundation (SNSF); United Kingdom – Department of Physics, University of Oxford.